Structural and Biochemical Insights into the Multiple Functions of Yeast Grx3

Chang-Biao Chi, YaJun Tang, Jiahai Zhang, Ya-Nan Dai, Mohnad Abdalla, Yuxing Chen and Cong-Zhao Zhou

School of Life Sciences and Hefei National Laboratory for Physical Sciences at the Microscale, *University of Science and Technology of China, Hefei, Anhui 230027, People's Republic of China*
Key Laboratory of Structural Biology, *Chinese Academy of Science, Hefei, Anhui, 230027, People's Republic of China*

Correspondence to YaJun Tang and Cong-Zhao Zhou: *School of Life Sciences and Hefei National Laboratory for Physical Sciences at the Microscale, University of Science and Technology of China, Hefei, Anhui 230027, People's Republic of China. tangyj@ustc.edu.cn; zcz@ustc.edu.cn*
https://doi.org/10.1016/j.jmb.2018.02.024
Edited by Charalampo Kalodimos

Abstract

The yeast *Saccharomyces cerevisiae* monothiol glutaredoxin Grx3 plays a key role in cellular defense against oxidative stress and more importantly, cooperates with BolA-like iron repressor of activation protein Fra2 to regulate the localization of the iron-sensing transcription factor Aft2. The interplay among Grx3, Fra2 and Aft2 responsible for the regulation of iron homeostasis has not been clearly described. Here we solved the crystal structures of the Trx domain ($Grx3^{Trx}$) and Grx domain ($Grx3^{Grx}$) of Grx3 in addition to the solution structure of Fra2. Structural analyses and activity assays indicated that the Trx domain also contributes to the glutathione *S*-transferase activity of Grx3, via an inter-domain disulfide bond between Cys37 and Cys176. NMR titration and pull-down assays combined with surface plasmon resonance experiments revealed that Fra2 could form a noncovalent heterodimer with Grx3 via an interface between the helix-turn-helix motif of Fra2 and the C-terminal segment of $Grx3^{Grx}$, different from the previously identified covalent heterodimer mediated by Fe–S cluster. Comparative affinity assays indicated that the interaction between Fra2 and Aft2 is much stronger than that between Grx3 and Aft2, or Aft2 toward its target DNA. These structural and biochemical analyses enabled us to propose a model how Grx3 executes multiple functions to coordinate the regulation of Aft2-controlled iron metabolism.

Introduction

Reactive oxygen species, which cause oxidative damage to biological macromolecules, are mainly generated in the process of mitochondrial oxidative phosphorylation and in response to exogenous compounds [1]. Living cells utilize regulatory proteins to maintain the redox states of oxidized macromolecules. Particularly, two groups of oxireductases, namely, glutaredoxins (Grxs) and thioredoxins (Trxs), are involved in the reduction and regeneration of oxidized proteins [2]. Compared to Trxs, Grxs are more versatile with respect to the choice of substrates and reaction mechanisms [1]. Grxs are thiol oxidoreductases, which require the reduced form of glutathione (GSH) as the electron donor to reduce the mixed disulfide.

The yeast *Saccharomyces cerevisiae* encodes three dithiol Grxs: Grx1, Grx2 and Grx8, in addition to five monothiol Grxs: Grx3, Grx4, Grx5, Grx6 and Grx7, which are of diverse functions [1,3–6]. The cytosolic monothiol Grxs Grx3 and Grx4 are highly homologous isoforms that belong to a subgroup of the Grxs featured with an N-terminal Trx domain followed by a C-terminal Grx domain [7]. The reductase activity of the Trx domain can be excluded, since the conserved attacking cysteine of the Trx active site is absent. In contrast, the Grx domain exhibits a typical monothiol Grx fold. However, it remains unclear whether there exists crosstalk between the two domains.

In addition, Grx3 and Grx4 participate in the regulation of iron metabolism [8]. It is known that iron is an essential element for all organisms, and its

intracellular homeostasis is important for the viability of cell. Excess iron is toxic to the cell because it generates free radicals that may oxidize and damage DNA, lipids and proteins [9,10]. In *S. cerevisiae*, transcription factor Aft2 regulates a subset of genes defined as the high-affinity iron-uptake regulon [11]. Under the condition of iron sufficiency, Grx3 forms a GSH ligated, Fe–S bridged heterdimer, which was proposed to transfer Fe–S cluster to Aft2 via Fra2 [12], an iron-responsive transcription regulatory protein that senses the cytosolic Fe–S cluster [13]. Formation of a stable heterodimer of Grx3 and Fra2 is necessary to promote the dissociation of Aft2 from the target DNA, leading to the down-regulation of Aft2 controlled genes [12]. On the other hand, under the condition of iron deficiency, Grx3 and Fra2 may also form a noncovalently linked heterodimer and leave Aft2 for the transcription of iron-uptake regulon [13]. Notably, iron deficiency is involved in several human diseases including anemia, neuronal and immunological alterations [14]. Nevertheless, the structural and biochemical insights into the crosstalk among Grx3, Fra2 and Aft2 are not clear.

Here we reported the crystal structures of both the Trx and Grx domains of yeast Grx3, which enabled us to model a full-length structure of Grx3 with an inter-domain disulfide bond. Despite the Trx domain alone losses the typical Trx activity, it significantly augments the glutathione *S*-transferases (GSTs) activity of the Grx domain, most likely via the inter-domain disulfide bond. The NMR structure of Fra2 combined with the titration and pull-down assays in addition to the surface plasmon resonance (SPR) experiments clearly assigned the interface between Fra2 and Grx3. Once Grx3 is captured by Fra2 in the cytosol, upon iron deficiency, Aft2 might be accumulated in the nucleus, and activate the expression of the downstream genes; whereas, upon the localization of [2Fe–2S]–Grx3–Fra2 heterodimer in the nucleus under the condition of iron sufficiency, Aft2 is dissociated from the target DNA, leading to the down-regulation of transcription. These findings provide the structural and biochemical insights into the multiple functions of Grx3 under different physiological conditions.

Results

Overall structure of yeast Grx3

Grx3 is composed of two segments, an N-terminal Trx domain (Met1–Ser114, $Grx3^{Trx}$), and a C-terminal Grx domain (Glu144–Ser250, $Grx3^{Grx}$), connected by a non-conserved linker (Fig. 1a). Each domain possesses a conserved cysteine, namely, Cys37 in Trx domain and Cys176 in Grx domain. The tandem organization of a Trx followed by a Grx domain of yeast Grx3 could be found in many other organisms. Although the primary sequences of the two individual domains are highly conserved (Figs. S1A and S2B), the linkers between two domains vary a lot not only in length but also in sequence.

We tried to solve the full-length structure of Grx3 but failed. Alternatively, we resolved the crystal structures of the two individual domains. The overall fold of the $Grx3^{Trx}$ (Fig. 1b) possesses a typical αβαβαββα topology of known Trx, very similar to the previously published Trx domain of Grx3 (PDB code 3D6I) [16], with an RMSD of 1.2 Å over 107 Cα atoms. Notably, the signature motif ($W^{33}AEP^{36}$), which is missing in the structure of 3D6I, could be clearly traced in our structure; moreover, the residue Cys37 is rather exposed and located at the loop region (Fig. 1c). Multiple-sequence alignment indicated that the yeast $Grx3^{Trx}$ and homologs all lacked the attacking cysteine residue at the active site (Fig. S1A), suggesting that they could not catalyze the disulfide bond reduction. As expected, we found that neither the full-length Grx3 nor $Grx3^{Trx}$ could reduce the disulfide bonds in insulin, using the insulin coupled with the NADPH-Trx reductase-Trx assays [17,18]. Interestingly, either individual Trx or Grx domain of Grx4 failed to rescue the *grx4* deletion cells with respect to cell growth [19]. It was suggested that $Grx3^{Trx}$ should need the assistant of $Grx3^{Grx}$ to complete the functions of Grx3.

The overall architecture of $Grx3^{Grx}$ employs the typical Grx fold: a core of four antiparallel β-strands surrounded by five α-helices. Strand β3 is antiparallel to the other three β-strands (β1, β2, β4) (Fig. 1d). Structural superposition of $Grx3^{Grx}$ with the second Grx domain of human Txnl2 yielded an overall RMSD of 1.4 Å over 98 Cα atoms (Fig. 1e). The $C^{176}GFS^{179}$ motif of Grx3 localizes at the N-terminus of helix α2 and the preceding loop. The putative GSH-binding motif (Arg205, Thr216–Phe217–Pro218, and Gly228–Gly229–LeU230–Asp231–Ile232) localizes at the middle of helix α3, the loop that precedes β3, and the loop that precedes helix α4 (Fig. S1B).

The interplay between the two domains of Grx3

Multiple-sequence alignment indicated that the catalytic cysteine and GSH-binding residues are conserved among all Grx domain of Grx3 and homologs from yeast and *Arabidopsis thaliana* to *Homo sapiens* (Fig. S1B). Structural analyses indicated that the Grx domain of Grx3 most likely possesses the bis-(2-hydroxyethyl) disulfide (HEDS) and GST activity. The HEDS activity of typical Grxs is usually detected through reducing the mixed disulfide of glutathionylated β-mercaptoethanol [20]. However, compared to typical dithiol Grxs, Grx3 possesses a very low HEDS activity, approximately only 1% to that of yeast Grx2.

GSTs belong to a family of enzymes mainly involved in the detoxification of xenobiotic compounds by conjugation to the sulfhydryl group of GSH, which is

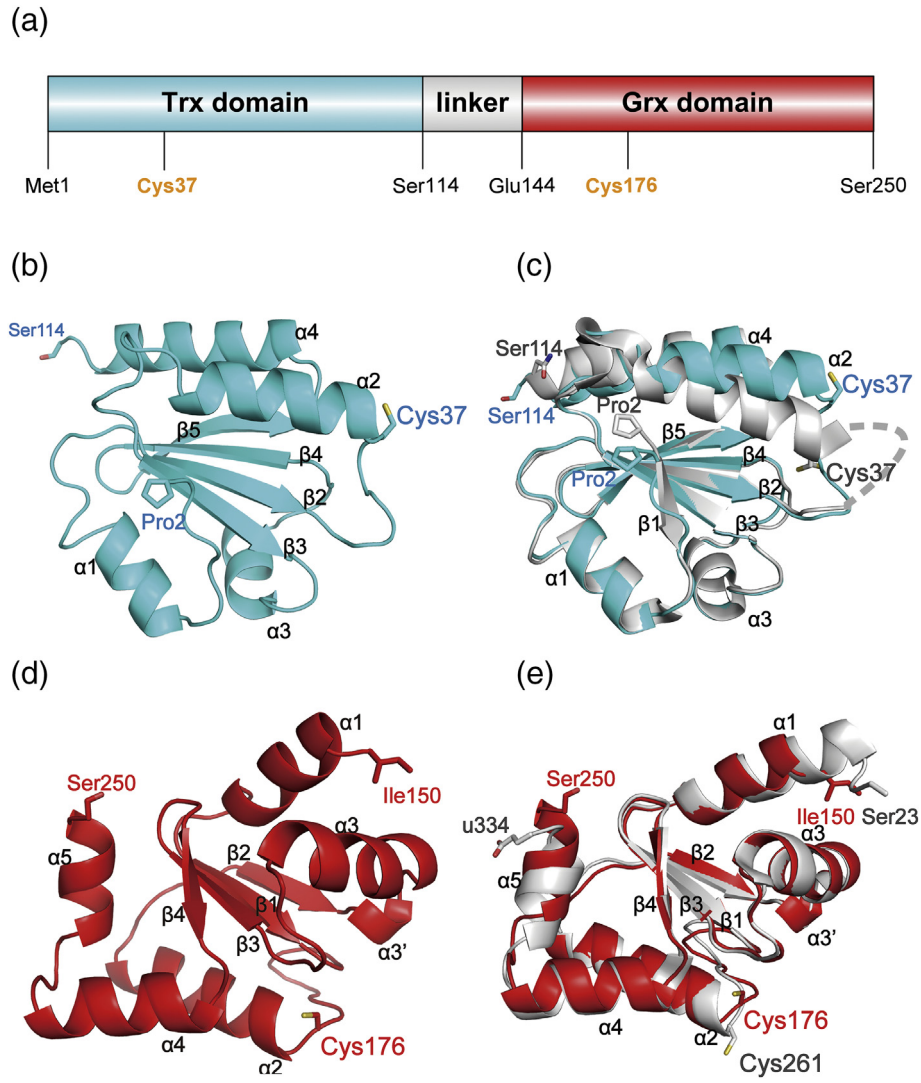

Fig. 1. Domain organization of yeast Grx3 and overall structure of the two dimains $Grx3^{Trx}$ and $Grx3^{Grx}$. (a) Domain organization of yeast Grx3. Three segments of Grx3 are drawn by Domain Graph, version 1.0 [15]. The Trx and Grx domains are shown in cyan and red, respectively. (b) Crystal structure of the Trx domain. (c) Structural superposition of $Grx3^{Trx}$ (sky blue) against the previously published Trx domain of Grx3 (3D6I) (gray). (d) Crystal structure of the Grx domain. (e) Structural superposition of $Grx3^{Grx}$ (red) against human TXNL2 (2yan) (gray).

activated to reactive thiolate form by residues around the active site [21]. With yeast Grx2 as the control [22], the GST activities of Grx3, $Grx3^{C37S}$ mutant, $Grx3^{Grx}$ and $Grx3^{Trx}$ were detected by monitoring the absorbance at 419 nm for the conversion of 4-chloro-7-nitro-2,1,3-benzox-adiazole (NBD-Cl; Sigma-Aldrich) to glutathionylated NBD. We found that Grx3 possesses GST activity at a catalytic velocity similar to that of yeast Grx2 (Fig. 2a), whereas the $Grx3^{C37S}$ mutant and $Grx3^{Grx}$ possess a GST activity of approximately 70% and 50% of Grx3, respectively. In contrast, $Grx3^{Trx}$ does not display any GST enzyme activity, indicating that the Trx domain could improve the GST activity of the Grx domain, most likely via the contribution of Cys37 (Fig. 2a).

Thus, we proposed that the two domains of Grx3 could crosstalk via a transient inter-domain disulfide bond. As we know, Grx3 has three cysteines: Cys37 and Cys108 in the Trx domain, in addition to Cys176 in the Grx domain. Multiple-sequence alignment (Fig. S1B) and the previous reports of Grx3 [23] indicated that Cys176 was the catalytic cysteines, whereas Cys37 in the Trx domain was also strictly conserved, leaving Cys108 totally non-conserved, which most likely not involved in the crosstalk. Cross-linking experiments between $Grx3^{Grx}$ and different mutants of $Grx3^{Trx}$ revealed that Cys176 of $Grx3^{Grx}$ form a disulfide bond with Cys37 of Trx^{C108S}, resulting a cross-linked Trx–Grx complex, which could be further reduced by DTT (Fig. 2b). However, no

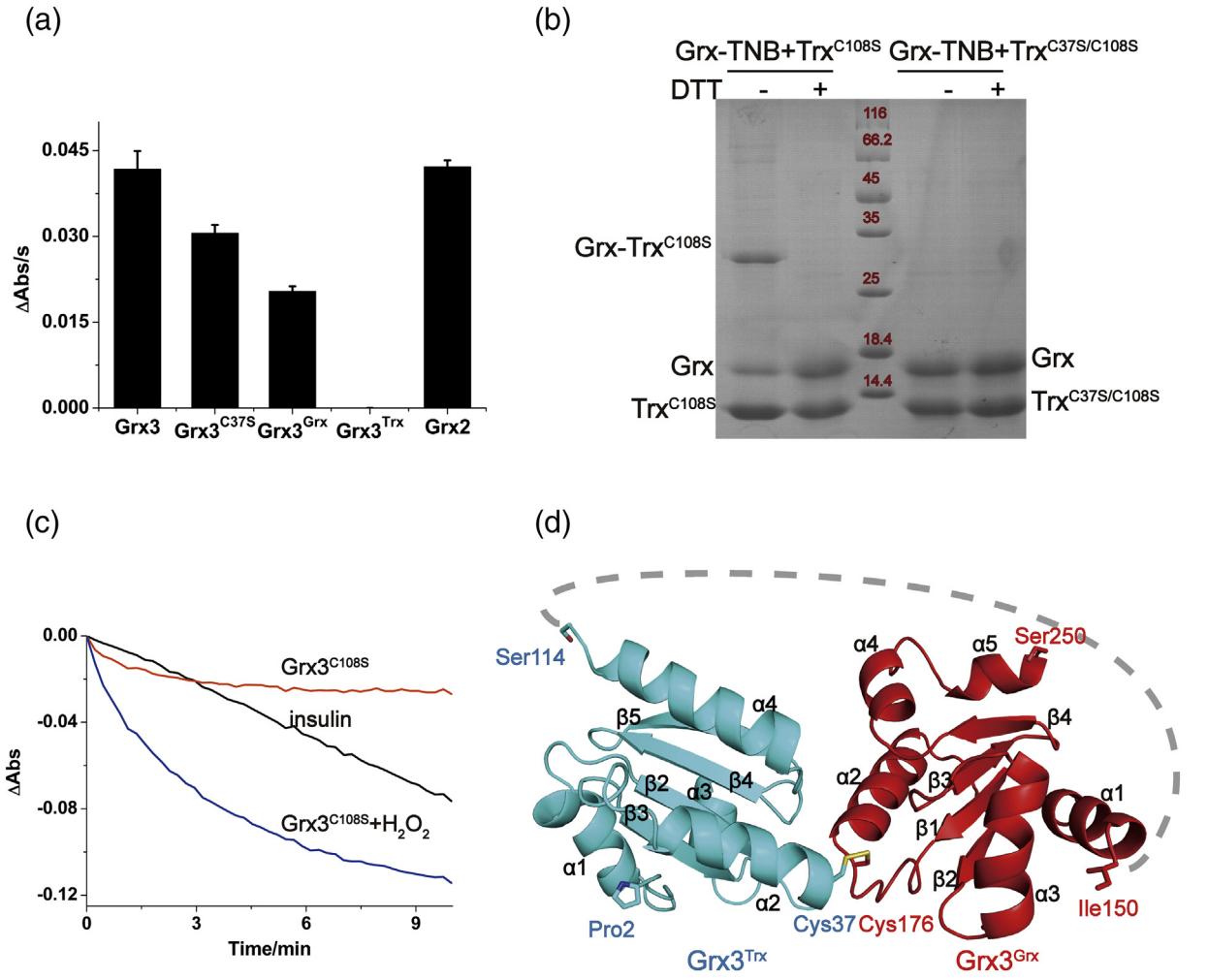

Fig. 2. The interplay between the two domains of Grx3. (a) GST activity assays of Grx3, Grx3^{C37S}, Grx3^{Grx}, Grx3^{Trx} and yeast Grx2. Assays were performed in 0.5 mM NBD-Cl, 2 mM GSH and the indicated enzyme at a final concentration of 10 μM. Shown are histograms of enzymatic activity. (b) Analyses of mixed disulfide bond in the cross-linking experiments between Grx domain and Trx mutants (Trx^{C108S} and Trx$^{C37S/C108S}$). (c) Reduction of the intramolecular disulfide bonds in Grx3^{C108S}. The NADPH-Trx reductase-Trx system was applied to reduce the intramolecular disulfide bonds in insulin, overexpressed Grx3^{C108S} and Grx3^{C108S} under H_2O_2 stress. (d) A docking model of the full-length Grx3.

covalently linked complex was observed for the mutant Trx$^{C37S/C108S}$ and Grx3^{Grx} (Fig. 2b). Therefore, it strongly indicated that the Cys176 of Grx3^{Grx} can be regenerated by Cys37 of Grx3^{Trx} via a transient disulfide bond exchange reaction. Moreover, we used the NADPH-Trx reductase-Trx assays to confirm the formation of an intramolecular disulfide bond within Grx3 *in vivo*. First, we overexpressed Grx3^{C108S} in

Fig. 3. Solution structure of Fra2. (a) Sequence alignment of Fra2. Secondary structure elements of Fra2 are shown at the top of alignment. The residues which serve as the Fe–S cluster ligands are depicted by red stars. The HTH motifs are depicted by red square. The sequences of Fra2 and homologs are from the following organisms: *Saccharomyces cerevisiae* S288C (Fra2, NP_010383.4), *Candida glabrata* CBS 138 (CgFra2, XP_447553.1), *Hanseniaspora osmophila* (HoFra2, OEJ80763.1), *Hanseniaspora valbyensis* NRRL Y-1626 (HvBolA, OBA27552.1), *Phialocephala subalpina* (PsBolA, CZR57600.1), *Fusarium oxysporum* Fo47 (FoBolA, EWZ47850.1), *Fusarium fujikuroi* IMI 58289 (FfBolA, CCT67348.1), *Arabidopsis thaliana* (AtBolA2, NP_568217.1) and *Leucosporidium creatinivorum* (LcBolA, ORY88823.1). (b) Two-dimensional $^{15}N-^{1}H$ HSQC spectrum of Fra2. (c) Stereo view of the 20 structures of lowest energy superimposed for best fit of the N, CO, and CA atoms of residues 40–52, 57–61, 71–102, 105–110 and 113–115. (d) Cartoon representation of the solution structure of Fra2. (e) Structural superposition of Fra2 (green) and AtBolA2 (2MM9) (gray).

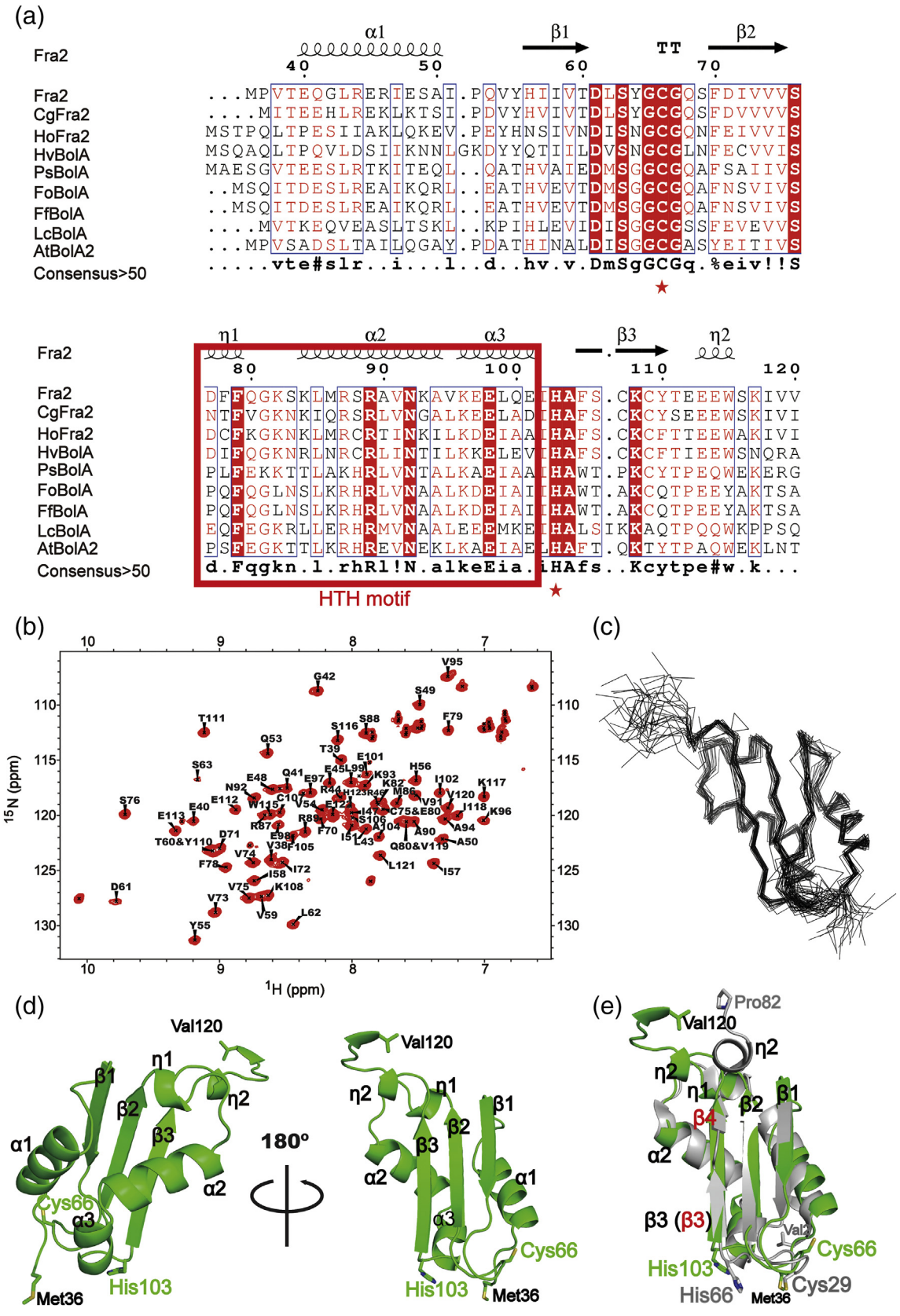

Fig. 3. (*legend on previous page*)

Escherichia coli under normal and H_2O_2 conditions, respectively. SDS-PAGE profiles excluded the formation of intermolecular disulfide bonds in $Grx3^{C108S}$ under both conditions (data not shown). Using insulin as the positive control of substrate, it is clear that $Grx3^{C108S}$ also possesses an intramolecular disulfide bond, which could be reduced by the Trx1–Trr1 system (Fig. 2c). These results enabled us to build a model of the interface between $Grx3^{Trx}$ and $Grx3^{Grx}$ using the HADDOCK web server (Fig. 2d). This model is similar to the previously reported structures of Trx–protein complexes [24–26]. It is likely the thiol group of Cys37 in $Grx3^{Trx}$, which is able to approach Cys176 in $Grx3^{Grx}$ and cleave the mixed disulfide bond to turn over $Grx3^{Grx}$.

NMR structure of Fra2 and its interaction with Grx3

To further investigate the interaction between yeast Fra2 and Grx3 during the process of Fe–S cluster transfer, we solved the NMR structure of Fra2 and clearly assigned the residues interacting with Grx3. Fra2, which belongs to the BolA family, is an iron-responsive transcription regulatory protein that senses the cytosolic Fe–S cluster [13]. There are two subfamilies of BolA: one with a conserved cysteine and another with two conserved histidines [27]. Multiple-sequence alignment indicated that Fra2 belongs to the former one (Fig. 3a). The ^{15}N–^{1}H heteronuclear single quantum coherence (HSQC) experiment showed a dispersed spectrum of amide groups (Fig. 3b), which indicated a well-folded structure. The structure of Fra2 was calculated using Xplor1.2. We determined and highly converged an ensemble of 20 structures of the lowest energy out of 200 calculated structures (Fig. 3c). RMSD of these 20 structures was 0.8 Å for the backbone atoms. The structural data and statistics are listed in Table 1.

Fra2 contains three β-strands and five α-helices with a topology of α1β1β2η1α2α3β3η2 (η stands for 3_{10} helix) (Fig. 3d). The conserved cysteine localizes at the loop between β1 and β2, which is the [H/C] loop in BolA proteins. Dali search indicated that the top 3 hits, which have a *Z* scores above 9.0, were all *A. thaliana* BolA2 (AtBolA2). However, compared with AtBolA2, local structural differences could be observed. Notably, the segment corresponding to the strand β3 in our Fra2 structure is split into two short strands β3 and β4 in AtBolA2 (Fig. 3e).

Under the iron-deficient condition, Fra2 could interact with Grx3 in a Fe–S cluster independent manner, which was supposed to facilitate the translocation of Aft2 into the nucleus [13]. However, the structural details of interaction remain unclear. To assign the residues at the interface, Grx3 was titrated against Fra2 sample. A series of ^{15}N–^{1}H HSQC spectra were recorded during the titration (Fig. 4a). A total of 14 resonances (Val73, Arg89, Ala90, Val91, Lys93, Ala94, Val95, Lys96, Glu97, Glu98, Ile102, Phe105, Ser106, Ile118) were observed to shift in a stepwise directional manner. Mapping the perturbed residues colored in yellow in the tertiary structure of Fra2 showed that they are mainly located at the HTH motif (α2α3) of Fra2 (Fig. 4e).

Previous studies have shown that *A. thaliana* GrxS14 interacts with BolA2 via a C-terminal segment of AtGrxS14 [27]. Residues involved in the interaction were located at the C-terminal segment from α3 to α4. Interestingly, the C-terminal segment α4 and α5 of *S. cerevisiae* Grx4 was reported to be essential for the regulation of Aft1 [19]. However, the fine interface between Fra2 and Grx3 (or Grx4) remains unclear. According to the titration results of *A. thaliana* GrxS14 against AtBolA2 [27], we designed the mutations of C-terminal segment in $Grx3^{Grx}$ [K209A/S212A/W214A (located at α3) and E215A/K234A/E235A (located at α4)] (colored in blue; Fig. 4e) and determined the binding affinities of the wild-type $Grx3^{Grx}$ and mutants toward Fra2 by SPR. The results showed that the dissociation constant (K_d) of the wild-type $Grx3^{Grx}$–Fra2 heterodimer is 30.5 ± 2.1 μM (Fig. 4b). Interestingly, the K_d value of mutant $Grx3^{Grx}$ (K209A/S212A/W214A) with Fra2 is 26.2 ± 5.2 μM (Fig. 4c), which is in

Table 1. Structural statistics for the 20 energy-refined conformers of Fra2

None of the structures exhibited distance violations of >0.5Å or dihedral angle violations of >5.r.m.s.d., root mean square violation.

Fra2	
NMR restraints	
NOE distance restraints	1372
Intra-residue	528
Sequential ($\|i-j\|=1$)	344
Medium range ($\|i-j\|<5$)	252
Long range ($\|i-j\|\geq 5$)	248
Hydrogen bonds	15
Dihedral angle restraints	37
Mean r.m.s.d. from idealized covalent geometry	
Bonds (Å)	0.002 ± 0.000
Angles (degrees)	0.379 ± 0.011
Improper (degrees)	0.266 ± 0.019
Mean r.m.s.d. from experiment restraints	
Distance (Å)	0.035 ± 0.003
Cdih (degree)	0.818 ± 0.137
Structural r.m.s.d. to the mean coordinates[a] (Å)	
Backbones atoms	0.8
Heavy atoms	1.5
Ramachandran plot analysis (%)[b]	
Residues in most favored regions	95.1
Residues in additional allowed regions	4.4
Residues in generously allowed regions	0.4
Residues in disallowed regions	0.1
Protein Data Bank entry	5Y4B

[a] Root mean square deviation was calculated using residues 40–52, 57–61, 71–102, 105–110 and 113–115, excluding the loop and disordered region.

[b] Ramachandran plot of ordered residues was analyzed by Program PROCHECK.

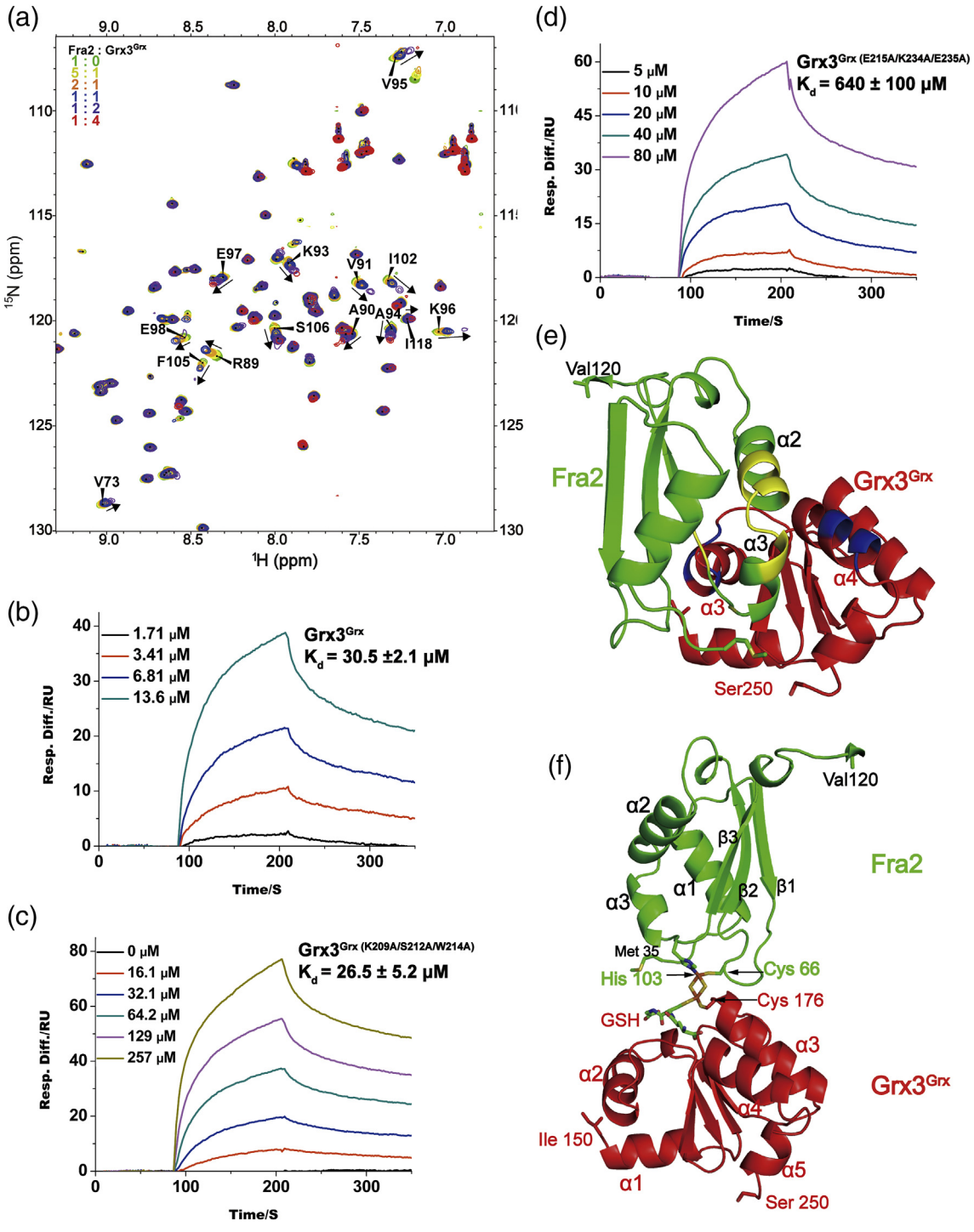

Fig. 4. Formation of Grx3^{Grx}–Fra2 complex. (a) The $^{15}N-^{1}H$ HSQC spectra showing significant chemical shift perturbations, which reflect the proposed interface residues. SPR assays analyze the interaction interface of (b) Grx3^{Grx}, (c) Grx3^{Grx} (K209A/S212A/W214A) and (d) Grx3^{Grx} (E215A/K234A/E235A) in Grx3^{Grx}–Fra2 heterodimer. Fra2 was immobilized on the surface of the CM5 chip. (e) The docking model of noncovalent Grx3^{Grx}–Fra2 heterodimer. (f) The docking model of [2Fe–2S]–Grx3^{Grx}–Fra2 heterodimer.

the same order of magnitude to the wild-type. However, the K_d value of Grx3^{Grx} (E215A/K234A/E235A) toward Fra2 reaches 640 ± 100 μM (Fig. 4d), showing a very low binding affinity. These results indicated that Grx3^{Grx} interacts with Fra2 via α4 rather than α3. It suggested that α4 of C-terminal region of Grx3^{Grx} is

involved not only in the physical interaction with Fra2 but also in the regulation of Aft1/2 [19]. Based on these results, we used HADDOCK webserver to build a model of $Grx3^{Grx}$–Fra2 heterodimer (Fig. 4e). The model showed that the interface is indeed formed by the C-terminal segment (mainly α4 helix) of $Grx3^{Grx}$ and the HTH motif of Fra2. Upon the iron deficiency, the C-terminal segment of $Grx3^{Grx}$ is occupied by Fra2, making it impossible to interact with Aft2.

A previous study identified a covalent interaction between Fra2 and $Grx3^{Grx}$ via [2Fe–2S] cluster [23]. A remarkable property of BolA is the capacity to form a heterodimer with Grx via a [2Fe–2S] cluster, all ligands of which have been well identified [27]. Moreover, the active-site Cys176 in Grx3, His103 in Fra2 and GSH has been identified as the Fe–S cluster ligands of [2Fe–2S]–Grx3–Fra2 heterodimers [28]. But the fourth ligand of Fe–S cluster remains unclear. From the known Fra2 structures, Cys66 of in the YGCG motif is the only conserved candidate residue in the [H/C] loop between β1 and β2 that is spatially close to the invariable His103 to coordinate an iron atom (Fig. 3d). A local conformation rearrangement of the [H/C] loop could place this cysteine at a proper position for serving as a [2Fe–2S] cluster ligand. In fact, the presence of a majority of small residues, such as glycines, guarantees the flexibility of this loop.

The crystal structure of *Coxiella burnetii* Co-BolA_H homodimer (PDB code 3TR3) revealed a cobalt atom ligated by two histidines from one monomer, mimicking the iron ligation [29]. In combination with our present structures of $Grx3^{Grx}$ and Fra2, a model for a [2Fe–2S]–$Grx3^{Grx}$–Fra2 heterodimer could be easily built (Fig. 4f). A rotation of Cys66 in Fra2 structures makes it possible to coordinate the iron atom via sulfur atom of Cys66 and the nitrogen atom of His103. Moreover, the docking [2Fe–2S]–$Grx3^{Grx}$–Fra2 heterodimer model showed that the HTH motif of Fra2 and C-terminal segment of Grx domain, which are important for the noncovalent interactions, are well exposed and independent of Fe–S cluster formation.

Competitive binding among Fra2, Aft2 and Grx3

As we know, Grx3 and Fra2 regulate the iron homeostasis via affecting the nuclear localization of Aft2 [8,13]. To validate the putative physical interactions between each pair of proteins of Fra2, Grx3 and Aft2, we first performed the pull-down assays. The His-tagged Fra2 or $Grx3^{Grx}$ was prepared as the bait pre-loaded to the Ni_2-NTA column, and the proteins Fra2 or the DNA-binding domain of Aft2 (residues Met1–Arg204, termed $Aft2^{1–204}$) without His-tag were loaded as the preys afterward. The results indicated that Fra2 and $Aft2^{1–204}$ could be pulled down by His-tagged $Grx3^{Grx}$ (Fig. S2A and S2B), whereas $Aft2^{1–204}$ could be pulled down by His-tagged Fra2 (Fig. S2C). Moreover, the absorbance spectra at 540 nm indicated that these three pairs of interactions are Fe–S cluster independent.

Furthermore, we applied SPR experiments to quantitatively analyze the pairwise binding affinity of Fra2, $Grx3^{Grx}$ and Aft2, in addition to the affinity of Aft2 toward its target DNA promoter, using fluorescence polarization assays. In the absence of a Fe–S cluster-mediated complex of Grx3 and Fra2, Aft2 binds to the *FET3* promoter, 5′-AAGTGCACCCATT-3′, to transcribe iron-uptake regulon genes [12]. SPR analyses showed that the K_d value of $Grx3^{Grx}$ toward $Aft2^{1–204}$ is 4.46 ± 1.22 μM (Fig. 5a), showing a much lower affinity compared to that of $Aft2^{1–204}$ toward the *FET3* promoter, which is 71 ± 14 nM (Fig. 5b). In contrast, Fra2 interacts with $Aft2^{1–204}$, at a K_d value of 33.8 ± 11.3 nM (Fig. 5c), a comparable affinity that enables Fra2 to compete with target DNA in binding Aft2. Although the nucleus-localized Grx3 contributes little to the release of Aft2 from the DNA, formation of a Fe–S cluster bridged heterodimer between Grx3 and Fra2 is indispensable for the translocation of Fra2 from cytosol to the nucleus to regulate the localization of Aft2 [12]. Notably, SPR analyses showed that the K_d values of Fra2 and Aft2 toward the full-length Grx3 are 14.6 ± 1.3 and 3.70 ± 0.51 μM, respectively (Figs. S3A and S3B), which are in the same order of magnitude to

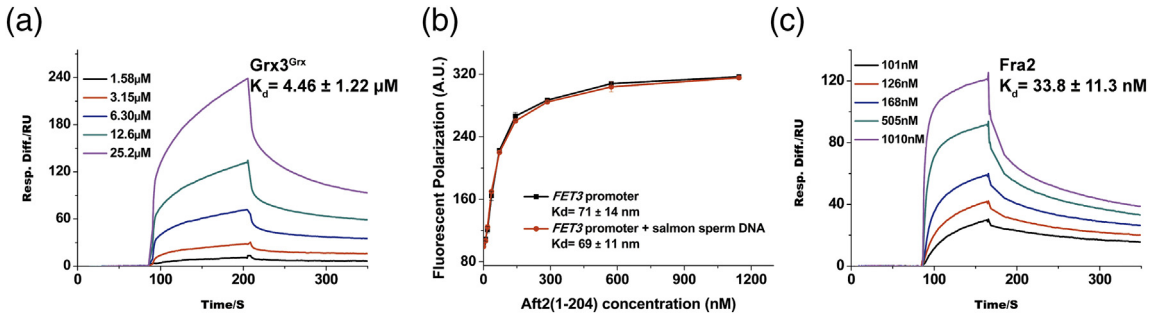

Fig. 5. Binding affinities of $Grx3^{Grx}$–Aft2, Aft2–DNA and Fra2–Aft2. (a) SPR experiments to analyze the binding affinity between $Grx3^{Grx}$ and Aft2. Aft2 was immobilized on the surface of the CM5 chip. (b) Fluorescence polarization assays to analyze the binding affinity between *FET3* promoter and Aft2. (c) SPR experiments to analyze the binding affinity between Fra2 and Aft2. Aft2 was immobilized on the surface of the CM5 chip.

that toward $Grx3^{Grx}$ (Figs. 4B or 5A). It indicated that the interactions with Fra2 and Aft2 are independent of the Trx domain of Grx3.

Discussion

Grx3 works as a GST upon oxidative stress

Due to iron's prooxidant property in generating free radicals (i.e., producing hydroxyl radicals from H_2O_2), iron-induced oxidative stress is a serious challenge to the cell [30]. Hydroxyl radicals are the most reactive radical oxygen species and are known to have the ability to react with cellular constituents and attack cell membrane lipids, causing lipid peroxidation [31]. During conditions of iron sufficiency, the excess of iron leads to oxidative stress of the cells. Previous study showed that the yeast *grx3grx4* double mutant was sensitive to oxidizing agents [8]. Moreover, deletion of *aft1* in the *grx3grx4* double mutant could not efficiently rescue the sensitivity to the oxidizing agent hydrogen peroxide [32], indicating that Grx3 and Grx4 might play additional roles in the oxidative stress response through proteins other than Aft1. This conclusion is supported by our result that Grx3 possesses the GST activity at a catalytic velocity similar to that of Grx2 (Fig. 2a). We propose that under the condition of iron sufficiency, Grx3 is capable of forwarding electrons from GSH or NADPH to a variety of oxidized substrates to fight against oxidative stress.

Interestingly, previous study showed that either individual Trx or Grx domain of Grx4 failed to rescue the *grx4* cells with respect to cell growth and the function of iron-dependent enzymes, but with gain of function once fused with a corresponding evolutionarily similar Grx or Trx domain [19]. Moreover, the Trx domain of Grx3 is also sufficient to promote cell survival in response to oxidative stress [32]. These results demonstrated that fused Trx domain is also essential for the *in vivo* function of the multidomain monothiol Grxs via inter-domain interactions, in agreement with the results of our GST activity assays and cross-linking experiments (Fig. 2a and b).

Grx3 cooperates with Fra2 to regulate the activity of Aft2

It has been reported that the interaction between Fra2 and Grx3/4 could modulate the Aft2 activity under both iron sufficiency and deficiency growth conditions [13,23]. Moreover, Grx3 is proposed to form a GSH ligated, Fe–S bridged homodimer to relay Fe–S cluster to Aft2, which eventually forms a heterodimer with Fra2 in the condition of iron sufficiency [11]. The rapid Fe–S cluster transfer reaction between Grx3–Fra2 and Aft2 clearly emphasizes the essential role of Fra2 in mediating the Fe–S cluster transfer from Grx3 to Aft2 [12]. However, the

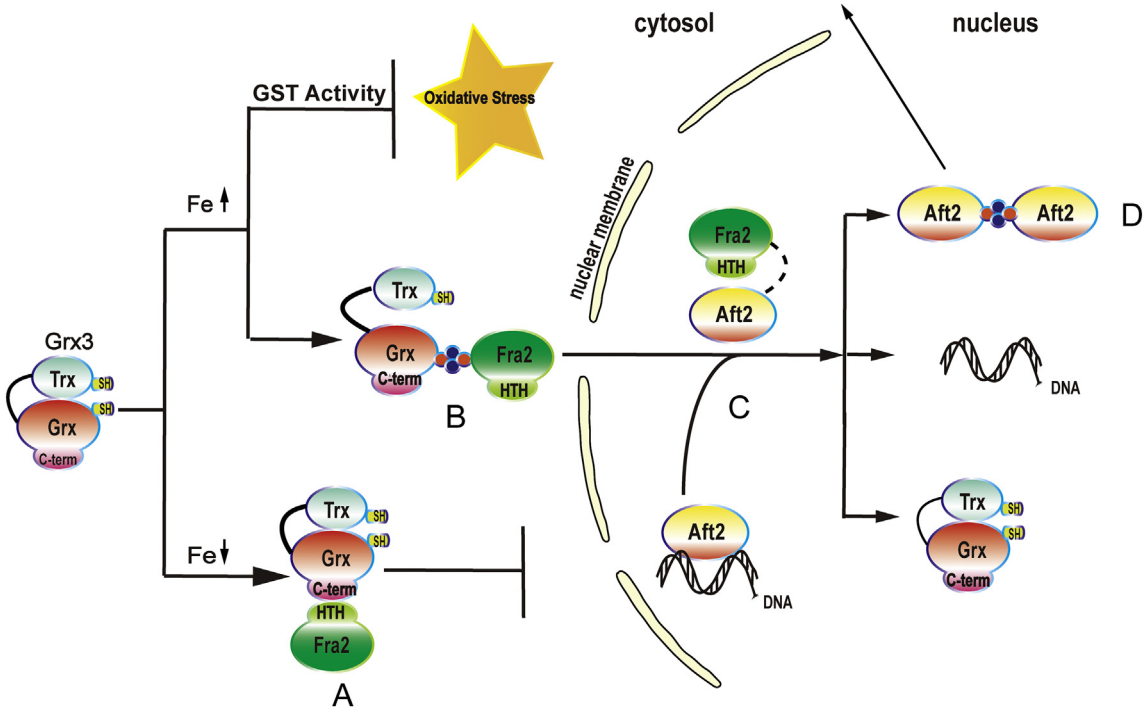

Fig. 6. A putative model of multiple functions of Grx3.

precise interface and regulatory mechanism remain unclear. Based on the structural and biochemical studies, here we propose a model on how Grx3 and Fra2 work together to coordinate the Aft2-controlled iron metabolism (Fig. 6).

In the condition of iron deficiency, Grx3 forms a noncovalent heterodimer with Fra2 (Fig. 6a), via an interface between the C-terminal segment of Grx3 and the HTH domain of Fra2. In agreement with our results, a previous report using a split YFP tagging of Fra2 or Grx4 revealed that noncovalent Grx4–Fra2 complex interaction could be detected in cells in iron deficiency conditions [13]. In addition, the fluorescence of Fra2–Grx4 complex appeared to be primarily cytosolic, and the distribution and levels of fluorescence were iron independent [13]. Thus, upon iron deficiency, the noncovalent Grx3–Fra2 complex sequesters Fra2 in the cytosol, making it impossible to interact with Aft2 in nucleus.

Under the condition of iron sufficiency, Grx3 executes at least two functions. On one hand, it functions as a GST to fight against oxidative stress, with an activity comparable to yeast Grx2 (Fig. 2a). On the other hand, it forms a heterodimer with Fra2, a dominantly cytosolic protein, mediated by a Fe–S cluster. In detail, the catalytic residues Cys176 of Grx3, Cys66 and His103 of Fra2, in addition to a GSH molecule serve as ligands of the [2Fe–2S] cluster (Fig. 6b), which is required for the inactivation of Aft2 *in vivo* [23,28]. Notably, we deduced from the NMR structure that Cys66 of Fra2 should serve as a ligand of the [2Fe–2S] cluster. Upon covalently binding to Grx3, Fra2 is translocated to the nucleus. Notably, a previous report has demonstrated that yeast Aft1 most likely recognizes a negatively charged region in the C-terminal segment of Grx4 [19]. Moreover, the exposed C-terminal segment of Grx3 is responsible for recruiting Aft2 and probably elevates the efficiency of Fe–S cluster transfer from Grx3–Fra2 to Aft2 [19,33]. Due to the much higher affinity between Fra2 and Aft2, the nucleus-localized Fra2 predominantly binds to Aft2 (Fig. 6c), with an unknown interface. In consequence, the [2Fe–2S] cluster is transferred from Grx3–Fra2 to Aft2, resulting in the release of Aft2 from the target DNA and the dimerization of Aft2 bridged by the [2Fe–2S] cluster (Fig. 6d). Finally, the transcription of Aft2-controlled genes, including iron-uptake regulon, is down-regulated, and dimerized Aft2 is exported to the cytosol by the exportin Msn5 [11,34], resulting in the shut-down of iron-uptake regulon expression.

Experimental Procedures

Construction, expression, and purification of Grx3, Fra2 and Aft2

The coding regions of yeast Grx3 (residues Met1–Ser250), Trx domain (residues Met1–Ser114), Grx domain (residues Glu144–Ser250), Fra2 (residues Met36–Val120) and Aft2 (residues Met1–Arg240) were amplified by PCR from the genomic DNA of *S. cerevisiae* S288C. A hexahistidine tag was added at the C-terminal of Grx3, Trx domain, Grx domain and Fra2. The PCR products were inserted into a pET28a-derived vector (Novagen) and transformed into *E. coli* strain BL21 (DE3) (Novagen). These cells were induced with 0.02 mM IPTG at 16 °C for 20 h after the OD_{600nm} reached 0.6. Cells were collected by centrifugation and resuspended in buffer A [20 mM Tris–HCl (pH 8.0), 100 mM NaCl]. After 30 min of sonication followed by centrifugation at 20,000*g* for 30 min, the supernatant was pooled and loaded onto a Ni-NTA column (GE Healthcare). The target proteins were eluted with 450 mM imidazole and loaded onto a Superdex 75 16/60 column preequilibrated with buffer A. The cloning and purification of Aft2 have been described previously [12].

Crystallization, data collection, structure solution, and refinement of Trx domain and Grx domain of Grx3

Fractions containing recombinant Trx domain and Grx domain were pooled, desalted and concentrated to 10 mg/mL in a final solution of 20 mM Tris–HCl (pH 8.0) and 100 mM NaCl for crystal screening. Protein crystals were grown at 16 °C in a hanging drop of 1.0 μL protein sample with an equal volume of reservoir solution. After about 3 days, prismatic crystals of Trx domain or Grx domain appeared in the 0.1 M Tris–HCl (pH 8.0) and 2 M ammonium sulfate. Microseeding was adopted for crystal optimization. A single crystal was transferred to cryoprotectant reservoir solution supplemented with 25% glycerol and flash-cooled with liquid nitrogen. X-ray diffraction data were collected at 100 K in a liquid nitrogen stream, using beamline BL17U with an ADSC Q315R CCD detector and beamline BL18U with a DECTRIS PILATUS 6M PIXEL detector at the Shanghai Synchrotron Radiation Facility. The data sets were processed and scaled using HKL2000 [35]. The initial models were further refined by manual and automatic rebuilding using molrep from the CCP4i program package [36]. We used the atomic coordinates of first Grx domain of *H. sapiens* GLRX3 as the search model (PDB code 3ZYW) to solve the structures of the Grx domain and atomic coordinates of the Trx domain of yeast Grx3 as the search model (PDB code 3D6I) to solve the structure of the Trx domain. The final model was obtained after several rounds of manual rebuilding and refinement using Coot and Refmac5 [37] from the CCP4i package [38], and checked using the program MolProbity [39] and PROCHECK [40]. Data collection and refinement statistics are listed in Table 2.

Table 2. Crystal parameters, data collection, and structure refinement

	$Grx3^{Trx}$	$Grx3^{Grx}$
Data collection		
Space group	$P4_12_12$	$P2_12_12_1$
Unit cell		
a, b, c (Å)	77.3, 77.3, 37.1	41.2, 45.7, 45.8
α, β, γ (°)	90.0, 90.0, 90.0	90.0, 90.0, 90.0
Resolution range (Å)	50.00–1.40 (1.45–1.40)[h]	50.00–1.70 (1.76–1.70)
Unique reflections	22,509 (2203)	9733 (967)
R_{merge}[a]	0.046 (0.616)	0.059 (0.398)
$I/\sigma I$	40.0 (2.8)	20.7 (3.0)
Completeness (%)	99.6 (99.8)	97.0 (98.8)
Average redundancy	6.9 (6.9)	4.2 (4.3)
Structure refinement		
Resolution range (Å)	34.58–1.40	25.46–1.70
R_{work}[b]/R_{free}[c]	0.188/0.219	0.180/0.229
Number of protein atoms	922	803
Number of water atoms	103	62
RMSD[d] bond lengths (Å)	0.030	0.019
RMSD bond angles (degrees)	2.409	1.844
Average *B*-factors (Å^2)		
Protein	20.3	23.1
Ramachandran plot[e] (residues, %)		
Most favored	97.39	100
Additional allowed	2.61	0.00
Outliers	0.00	0.00
MolProbity clashscore[f]/score percentile	6.51/82nd percentile (N = 480, 1.40 ± 0.25 Å)	1.25/99th percentile (N = 819, 1.70 ± 0.25 Å)
MolProbity score[g]/score percentile	1.48/84th percentile (N = 3363, 1.40 ± 0.25 Å)	0.85/100th percentile (N = 9248, 2.35 ± 0.25 Å)
Protein Data Bank entry	5Y4T	5Y4U

[a] $R_{merge} = \sum_{hkl}\sum_i |I_i(hkl) - <I(hkl)>| / \sum_{hkl}\sum_i I_i(hkl)$, where $I_i(hkl)$ is the intensity of an observation and $<I(hkl)>$ is the mean value for its unique reflection. Summations are over all reflections.
[b] $R_{work} = \sum_h |F_o(h) - F_c(h)| / \sum_h F_o(h)$, where F_o and F_c are the observed and calculated structure factor amplitudes, respectively.
[c] R_{free} was calculated with 5% of the data excluded from the refinement.
[d] RMSD, root mean square deviation from ideal values.
[e] The categories were defined by Molprobity.
[f] The number of serious steric overlaps (>0.4 Å) per 1000 atoms.
[g] MolProbity score combines the clashscore, rotamer and Ramachandran evaluations into a single score, normalized to be on the same scale as X-ray resolution.
[h] The values in parentheses refer to statistics in the highest bin.

NMR spectroscopy, data processing, structure calculation and validation

Both ^{15}N-labeled and $^{15}N/^{13}C$-labeled Fra2 samples were dissolved to a final concentration of 0.8 mM in 500 µL buffer containing 50 mM phosphate sodium (pH 8.0), 150 mM NaCl and 5 mM DTT in a 90% H_2O and 10% D_2O mixture or in 99.96% D_2O. All NMR experiments were carried out at 303 K on Bruker DMX600 spectrometer. The following spectra were recorded with self-shielded-axis gradients to obtain the backbone and side-chain resonance assignments: 2D $^{15}N-^1H$ HSQC and 3D HNCO, HN(CA)CO, CBCA(CO)–NH, CBCANH, (H)C(CO)NH–TOCSY, HBHA(CBCA)–(CO)NH, H(C)(CO)NH–TOCSY, HCCH–COSY, and HCCH–TOCSY. The ^{15}N-labeled Fra2 was lyophilized and dissolved in 99.96% D_2O. A series of HSQC spectra were immediately collected to record the disappearance of NH signals and identify the slowly exchanging amides. NMR data were then processed using NMRPipe and NMRDraw [41], and analyzed with Sparky3 [42].

For NMR titration experiments, unlabeled Grx3 was prepared with a final concentration of 7 mM and the buffer contains 50 mM phosphate sodium (pH 8.0), 150 mM NaCl and 5 mM DTT. Titration experiments were performed by adding increasing amounts of unlabeled Grx3 to uniformly ^{15}N-labeled Fra2. A series of $^{15}N-^1H$ HSQC spectra were recorded at Fra2/Grx3 mole ratios of 5:1, 2:1, 1: 1, 1:2 and 1:4.

The NMR structures of Fra2 were calculated using Xplor1.2 program [43] with 1372 nuclear Overhauser effect (NOE) distance restraints, 37 backbone dihedral angle restraints and 15 hydrogen bond restraints. NOE distance restraints were obtained from 3D ^{15}N- and ^{13}C-edited NOE spectroscopy spectra. Backbone dihedral angle restraints (ϕ and ψ) of secondary structures were derived from the analysis of $^{13}C\alpha$, $^{13}C\beta$, ^{13}CO, $^1H\alpha$ and ^{15}N chemical shifts using program TALOS [44]. Hydrogen bond restraints were inferred from the slow-exchanging amide protons in the

secondary-structure regions. In the initial step of calculation, unambiguous NOE distance restraints of the sequential, medium-range and dihedral angle restraints were introduced. Then the hydrogen bonds and long-range NOEs were added into the calculation files. In the final stage, 200 structures were generated and the 20 structures with the lowest energies were collected to form the representative ensemble. Structural quality was further analyzed by PROCHECK [45]. Molecular graphics were visualized by PyMOL (http://www.pymol.org).

GST activity assays

GST activity was assayed according to the method of Ricci *et al.* [46], which follows the conjugation of NBD-Cl (Sigma-Aldrich) with GSH catalyzed by GST and produces a stable yellow compound with a strong absorbance at 419 nm. Stock solutions of 100 mM NBD-Cl and 100 mM GSH were freshly prepared. The assay mixture contained 0.5 mM NBD-Cl and 2 mM GSH. The final concentration of enzyme was 10 μM. The assay was started by the addition of NBD-Cl and monitored at 419 nm with a DU800 UV-visible spectrophotometer (Beckman Coulter) at 35 °C.

NADPH-Trx reductase-Trx assays

NADPH-Trx reductase-Trx assays was assayed according to the method of Holmgren and Bjornstedt [47], It was measured by reduction of the disulfide bonds of protein substrates. Stock solutions of 2 mg/mL NADPH, 1 M EDTA and 200 μM protein substrates (insulin, $Grx3^{C108S}$ and $Grx3^{C108S}$ over-expreessed under H_2O_2 conditions) were freshly prepared in 0.1M Tris–HCl (pH 7.5). The reaction mix contained 17.8 μM protein substrate, 85 μg/mL NADPH, 0.2 M EDTA, 8.33 nm Trr1 and 5 μM Trx1. Protein substrate, NADPH and EDTA were preincubated for 2 min before Trr1 was added. The assay was triggered by the addition of Trx1 and monitored at 340 nm with a DU800 UV–visible spectrophotometer (Beckman Coulter) at 37 °C.

Analyses of mixed disulfide bond formed between Grx domain and Trx domain mutants in crosslinking experiments

The complex linked with a disulfide bond was prepared according to the previous report [48]. Trx^{C108S}, $Trx^{C37S/C108S}$ and Grx domain were purified and reduced by DTT separately before desalting. Then, Grx domain was incubated with 20-fold molar excess of 5,5′-di-thiobis-(2-nitrobenzoicacid) at 25 °C to form a mixed disulfide between the active-site Cys176 of Grx domain and thionitrobenzoic acid. After desalting, two samples were prepared (A, 8 μM Grx domain + 16 μM Trx^{C108S}; B, 8 μM Grx domain + 16 μM $Trx^{C37S/C108S}$) and incubated at 25 °C for 30 min. Each sample was divided into two parts, with or without 5 mM DTT, and subjected to SDS-PAGE to test the quantity of the complex.

SPR assays

SPR assays were performed as previously described using a BIAcore 3000 instrument (GE Healthcare) [49]. The target protein in 10 mM sodium acetate (pH 5.0) was immobilized to flow cell 4 on the surface of the commercially available carboxymethyl dextran-coated substrates (CM5 chips; GE Healthcare) at a level of approximately 1000 resonance units. The sensor chip was washed and equilibrated in SPR buffer [20 mM Tris–HCl (pH 8.0), 150 mM NaCl, 1 mM DTT] containing 1 M potassium acetate at 298 K. The flow rate was 30 μL/min to minimize the mass transfer effect. SPR buffer was used as negative controls. Another protein in SPR buffer was injected into flow cells 3 and 4 of the sensor chip for 120 s and dissociated for 300 s. To regenerate the sensor chip, the bound material was completely removed by injecting 10 mM glycinate hydrochloride (pH 2.0). The signal of flow cell 4 was subtracted from that of flow cell 3 to eliminate nonspecific interactions. The sensorgrams were analyzed using BIA evaluation software (GE Healthcare). A Langmuir (1:1) binding model was used to analyze association rate constant k_{on} (M^{-1} s^{-1}) and dissociation rate constant k_{off} (s^{-1}). Dissociation constant K_d was also determined as the ratio of k_{off} and k_{on} ($K_d = k_{off}/k_{on}$) and represented by the mean ± standard error of three independent measurements.

Fluorescence polarization assays

This protein stock was diluted in 1/2 series in Buffer A [20 mM Tris–HC, (pH 8.0), 150 mM NaCl, 1 mM DTT) to 100 μM. The FAM-labeled double-stranded DNA probe stock was diluted to 100 nM in Buffer A. One hundred microliters of this diluted DNA probe was mixed with 100 μL of 1/2 series protein stock and incubated for 30 min. The fluorescence polarization was measured using a SpectraMax M5 plate reader (Molecular Devices) at 20 °C. Curves were fit individually using the equation [mP] = [maximum mP] × [C]/(K_d + [C]) + [baseline mP], where mP is millipolarization and [C] is protein concentration. K_d values and the fitting figures were derived (from three experimental replicates) by fitting the experimental data to the equation employing a fitting script written in python.

Accession numbers

Structural coordinates of yeast $Grx3^{Trx}$, $Grx3^{Grx}$ and Fra2 have been deposited in the Protein Data Bank, respectively (PDB IDs: 5Y4T, 5Y4U and 5Y4B).

Acknowledgments

We thank the staff at the Shanghai Synchrotron Radiation Facility and the Core Facility Center for Life Sciences at University of Science and Technology of China for technical assistance. This work is supported by the Ministry of Science and Technology of China (http://www.most.gov.cn, Grant No. 2012CB911002) and National Natural Science Foundation (http://www.nsfc.gov.cn, Grant No. 31400629).

Author Contributions: C.Z.Z. and Y.C. conceived, designed and supervised the project. C.Z.Z., Y.J.T. and C.B.C. analyzed data and wrote the manuscript. C.B.C., M.A. and Y.J.T. did the protein purification, crystal screening and optimization and physiological experiment. Y.J.T., J.H.Z. and C.B.C. performed NMR spectroscopy, data processing, NMR structure calculation and validation. All authors discussed the data and read the manuscript.

Conflict of Interest Statement: The authors declare that they have no conflicts of interest with the contents of this article.

Appendix A. Supplementary data

Supplementary data to this article can be found online at https://doi.org/10.1016/j.jmb.2018.02.024.

Received 30 November 2017;
Received in revised form 6 February 2018;
Accepted 27 February 2018
Available online 7 March 2018

Keywords:
oxidative stress;
Grx enzyme activity;
iron homeostasis;
surface plasmon resonance experiments;
the interaction analyses

Abbreviations used:
Grxs, glutaredoxins; Trxs, thioredoxins; GSH, glutathione; GSTs, glutathione *S*-transferases; SPR, surface plasmon resonance; HEDS, bis-(2-hydroxyethyl) disulfide; NBD-Cl, 4-chloro-7-nitro-2,1,3-benzox-adiazole; HSQC, heteronuclear single quantum coherence; NOE, nuclear Overhauser effect.

References

[1] E. Herrero, G. Belli, C. Casas, Structural and functional diversity of glutaredoxins in yeast, Curr. Protein Pept. Sci. 11 (2010) 659–668.

[2] C.M. Grant, Role of the glutathione/glutaredoxin and thioredoxin systems in yeast growth and response to stress conditions, Mol. Microbiol. 39 (2001) 533–541.

[3] J. Yu, N.N. Zhang, P.D. Yin, P.X. Cui, C.Z. Zhou, Glutathionylation-triggered conformational changes of glutaredoxin Grx1 from the yeast *Saccharomyces cerevisiae*, Proteins: Struct., Funct., Bioinf. 72 (2008) 1077–1083.

[4] W.-F. Li, J. Yu, X.-X. Ma, Y.-B. Teng, M. Luo, Y.-J. Tang, et al., Structural basis for the different activities of yeast Grx1 and Grx2, Biochim. Biophys. Acta 1804 (2010) 1542–1547.

[5] M. Abdalla, Y.-N. Dai, C.-B. Chi, W. Cheng, D.-D. Cao, K. Zhou, et al., Crystal structure of yeast monothiol glutaredoxin Grx6 in complex with a glutathione-coordinated [2Fe–2S] cluster, Acta Crystallogr. Sect. F: Struct. Biol. Commun. 72 (2016) 732–737.

[6] Y. Tang, J. Zhang, J. Yu, L. Xu, J. Wu, C.-Z. Zhou, et al., Structure-guided activity enhancement and catalytic mechanism of yeast grx8, Biochemistry 53 (2014) 2185–2196.

[7] C.H. Lillig, C. Berndt, A. Holmgren, Glutaredoxin systems, Biochim. Biophys. Acta 1780 (2008) 1304–1317.

[8] N. Pujol-Carrion, G. Belli, E. Herrero, A. Nogues, M.A. de la Torre-Ruiz, Glutaredoxins Grx3 and Grx4 regulate nuclear localisation of Aft1 and the oxidative stress response in *Saccharomyces cerevisiae*, J. Cell Sci. 119 (2006) 4554–4564.

[9] G. Papanikolaou, K. Pantopoulos, Iron metabolism and toxicity, Toxicol. Appl. Pharmacol. 202 (2005) 199–211.

[10] S. Puntarulo, Iron, oxidative stress and human health, Mol. Asp. Med. 26 (2005) 299–312.

[11] H. Li, C.E. Outten, Monothiol CGFS glutaredoxins and BolA-like proteins: [2Fe–2S] binding partners in iron homeostasis, Biochemistry 51 (2012) 4377–4389.

[12] C.B. Poor, S.V. Wegner, H. Li, A.C. Dlouhy, J.P. Schuermann, R. Sanishvili, et al., Molecular mechanism and structure of the *Saccharomyces cerevisiae* iron regulator Aft2, Proc. Natl. Acad. Sci. U. S. A. 111 (2014) 4043–4048.

[13] A. Kumanovics, O.S. Chen, L. Li, D. Bagley, E.M. Adkins, H. Lin, et al., Identification of FRA1 and FRA2 as genes involved in regulating the yeast iron regulon in response to decreased mitochondrial iron-sulfur cluster synthesis, J. Biol. Chem. 283 (2008) 10276–10286.

[14] J.L. Beard, Iron biology in immune function, muscle metabolism and neuronal functioning, J. Nutr. 131 (2001) 568–580.

[15] J. Ren, L. Wen, X. Gao, C. Jin, Y. Xue, X. Yao, DOG 1.0: illustrator of protein domain structures, Cell Res. 19 (2009) 271.

[16] L.M. Gibson, N.N. Dingra, C.E. Outten, L. Lebioda, Structure of the thioredoxin-like domain of yeast glutaredoxin 3, Acta Crystallogr. Sect. D: Biol. Crystallogr. 64 (2008) 927–932.

[17] A. Holmgren, Thioredoxin catalyzes the reduction of insulin disulfides by dithiothreitol and dihydrolipoamide, J. Biol. Chem. 254 (1979) 9627–9632.

[18] A. Holmgren, Reduction of disulfides by thioredoxin. Exceptional reactivity of insulin and suggested functions of thioredoxin in mechanism of hormone action, J. Biol. Chem. 254 (1979) 9113–9119.

[19] B. Hoffmann, M.A. Uzarska, C. Berndt, J.R. Godoy, P. Haunhorst, C.H. Lillig, et al., The multidomain thioredoxin-monothiol glutaredoxins represent a distinct functional group, Antioxid. Redox Signal. 15 (2011) 19–30.

[20] A. Holmgren, F. Aslund, [29] Glutaredoxin, Methods Enzymol. 252 (1995) 283–292.

[21] D. Sheehan, G. Meade, V.M. Foley, Structure, function and evolution of glutathione transferases: implications for

classification of non-mammalian members of an ancient enzyme superfamily, Biochem. J. 360 (2001) 1–16.
[22] M. Luo, Y.L. Jiang, X.X. Ma, Y.J. Tang, Y.X. He, J. Yu, et al., Structural and biochemical characterization yeast monothiol glutaredoxin Grx6, J. Mol. Biol. 398 (2010) 614–622.
[23] H. Li, D.T. Mapolelo, N.N. Dingra, S.G. Naik, N.S. Lees, B.M. Hoffman, et al., The yeast iron regulatory proteins Grx3/4 and Fra2 form heterodimeric complexes containing a [2Fe–2S] cluster with cysteinyl and histidyl ligation, Biochemistry 48 (2009) 9569–9581.
[24] Y. Li, Y. Hu, X. Zhang, H. Xu, E. Lescop, B. Xia, et al., Conformational fluctuations coupled to the thiol-disulfide transfer between thioredoxin and arsenate reductase in Bacillus subtilis, J. Biol. Chem. 282 (2007) 11078–11083.
[25] X.X. Ma, P.C. Guo, W.W. Shi, M. Luo, X.F. Tan, Y. Chen, et al., Structural plasticity of the thioredoxin recognition site of yeast methionine S-sulfoxide reductase Mxr1, J. Biol. Chem. 286 (2011) 13430–13437.
[26] S. Dai, R. Friemann, D.A. Glauser, F. Bourquin, W. Manieri, P. Schürmann, et al., Structural snapshots along the reaction pathway of ferredoxin–thioredoxin reductase, Nature 448 (2007) 92–96.
[27] T. Roret, P. Tsan, J. Couturier, B. Zhang, M.K. Johnson, N. Rouhier, et al., Structural and spectroscopic insights into BolA–glutaredoxin complexes, J. Biol. Chem. 289 (2014) 24588–24598.
[28] H. Li, D.T. Mapolelo, N.N. Dingra, G. Keller, P.J. Riggs-Gelasco, D.R. Winge, et al., Histidine 103 in Fra2 is an iron-sulfur cluster ligand in the [2Fe–2S] Fra2–Grx3 complex and is required for in vivo iron signaling in yeast, J. Biol. Chem. 286 (2011) 867–876.
[29] M.C. Franklin, J. Cheung, M.J. Rudolph, F. Burshteyn, M. Cassidy, E. Gary, et al., Structural genomics for drug design against the pathogen *Coxiella burnetii*, Proteins: Struct., Funct., Bioinf. 83 (2015) 2124–2136.
[30] B. Halliwell, J.M. Gutteridge, Oxygen free radicals and iron in relation to biology and medicine: some problems and concepts, Arch. Biochem. Biophys. 246 (1986) 501–514.
[31] M.B. Reddy, L. Clark, Iron, oxidative stress, and disease risk, Nutr. Rev. 62 (2004) 120–124.
[32] N. Pujol-Carrion, M.A. de la Torre-Ruiz, Glutaredoxins Grx4 and Grx3 of *Saccharomyces cerevisiae* play a role in actin dynamics through their Trx domains, which contributes to oxidative stress resistance, Appl. Environ. Microbiol. 76 (2010) 7826–7835.
[33] L. Ojeda, G. Keller, U. Muhlenhoff, J.C. Rutherford, R. Lill, D.R. Winge, Role of glutaredoxin-3 and glutaredoxin-4 in the iron regulation of the Aft1 transcriptional activator in *Saccharomyces cerevisiae*, J. Biol. Chem. 281 (2006) 17661–17669.
[34] R. Ueta, N. Fujiwara, K. Iwai, Y. Yamaguchi-Iwai, Mechanism underlying the iron-dependent nuclear export of the iron-responsive transcription factor Aft1p in *Saccharomyces cerevisiae*, Mol. Biol. Cell 18 (2007) 2980–2990.
[35] Z. Otwinowski, W. Minor, Processing of X-ray diffraction data collected in oscillation mode, Macromol. Crystallogr. Part A 276 (1997) 307–326.
[36] P. Emsley, K. Cowtan, Coot: model-building tools for molecular graphics, Acta Crystallogr. Sect. D: Biol. Crystallogr. 60 (2004) 2126–2132.
[37] G.N. Murshudov, A.A. Vagin, E.J. Dodson, Refinement of macromolecular structures by the maximum-likelihood method, Acta Crystallogr. Sect. D: Biol. Crystallogr. 53 (1997) 240–255.
[38] Collaborative CP, The CCP4 suite: programs for protein crystallography, Acta Crystallogr. Sect. D: Biol. Crystallogr. 50 (1994) 760.
[39] I.W. Davis, A. Leaver-Fay, V.B. Chen, J.N. Block, G.J. Kapral, X. Wang, et al., MolProbity: all-atom contacts and structure validation for proteins and nucleic acids, Nucleic Acids Res. 35 (2007) 375–383.
[40] R.A. Laskowski, M.W. Macarthur, D.S. Moss, J.M. Thornton, PROCHECK: a program to check the stereochemical quality of protein structures, J. Appl. Crystallogr. 26 (1993) 283–291.
[41] F. Delaglio, S. Grzesiek, G.W. Vuister, G. Zhu, J. Pfeifer, A. Bax, NMRPipe: a multidimensional spectral processing system based on UNIX pipes, J. Biomol. NMR 6 (1995) 277–293.
[42] R.D. Bellman, M.A. Holgate, T.G. Sugar, SPARKy 3: design of an active robotic ankle prosthesis with two actuated degrees of freedom using regenerative kinetics, Biomedical Robotics and Biomechatronics, 2008 BioRob 2008 2nd IEEE RAS & EMBS International Conference on: IEEE 2008, pp. 511–516.
[43] A.T. Brünger, P.D. Adams, G.M. Clore, W.L. Delano, P. Gros, R.W. Grosse-Kunstleve, et al., Crystallography & NMR system: a new software suite for macromolecular structure determination, Acta Crystallogr. Sect. D: Biol. Crystallogr. 54 (1998) 905–921.
[44] Y. Shen, F. Delaglio, G. Cornilescu, A. Bax, TALOS+: a hybrid method for predicting protein backbone torsion angles from NMR chemical shifts, J. Biomol. NMR 44 (2009) 213–223.
[45] R.A. Laskowski, J.A.C. Rullmann, M.W. Macarthur, R. Kaptein, J.M. Thornton, AQUA and PROCHECK-NMR: programs for checking the quality of protein structures solved by NMR, J. Biomol. NMR 8 (1996) 477–486.
[46] G. Ricci, A.M. Caccuri, M. Lobello, A. Pastore, F. Piemonte, G. Federici, Colorimetric and fluorometric assays of glutathione transferase based on 7-chloro-4-nitrobenzo-2-oxa-1, 3-diazole, Anal. Biochem. 218 (1994) 463–465.
[47] A. Holmgren, M. Bjornstedt, [21] Thioredoxin and thioredoxin reductase, Methods Enzymol, Elsevier 1995, pp. 199–208.
[48] P.-F. Wang, D.M. Veine, S.H. Ahn, C.H. Williams, A stable mixed disulfide between thioredoxin reductase and its substrate, thioredoxin: preparation and characterization, Biochemistry 35 (1996) 4812–4819.
[49] J. Homola, S.S. Yee, G. Gauglitz, Surface plasmon resonance sensors: review, Sensors Actuators B Chem. 54 (1999) 3–15.